Revealing the intrinsic superconducting gap anisotropy in surface-neutralized $BaFe_2(As_{0.7}P_{0.3})_2$

Ziming Xin
Peking University
Yudi Wang
Peking University
Cong Cai
Peking University
Zhengguo Wang
Peking University
Lei Chen
Peking University
Tingting Han
Peking University https://orcid.org/0000-0002-6052-7520
Yan Zhang (yzhang85@pku.edu.cn)
Peking University https://orcid.org/0000-0002-4979-4230

Article

Keywords: alkaline-earth iron arsenide (122), superconductors, complicacy, charge-non-neutral cleavage surface

Posted Date: August 20th, 2020

DOI: https://doi.org/10.21203/rs.3.rs-51914/v1

Version of Record: A version of this preprint was published at Communications Physics on February 19th, 2021. See the published version at https://doi.org/10.1038/s42005-021-00537-z.

Abstract

Alkaline-earth iron arsenide (122) is one of the most studied families of iron-based superconductors, especially for angle-resolved photoemission spectroscopy. Extensive results have been obtained including band structure, gap anisotropy, etc. However, the complicacy of 122 caused by its charge-non-neutral cleavage surface is rarely considered. Here, we show that the surface of 122 can be neutralized by potassium deposition. In potassium-coated $BaFe_2(As_{0.7}P_{0.3})_2$, the surface-induced spectral broadening is strongly suppressed, while the coherent spectra that reflects the intrinsic bulk electronic state recovers. This raises the accuracy of the gap measurement and gap fitting to an unpreceded level. The results clearly distinguish two pairing channels originated respectively from the inner and outer Fermi pockets. While the gap anisotropy on the outer hole/electron pockets can be well fitted using an s± gap function, the gap magnitude on the inner hole/electron pockets show a clear deviation. Our results provide quantitative constraints for refining theoretical models and demonstrate an experimental method for revealing the intrinsic electronic properties of 122 in future studies.

Introduction

After the discovery of superconductivity in $LaO_{1-x}F_xFeAs$ (1111), many families of iron-based superconductor have been found, including iron-selenide (11), alkaline iron arsenide (111), alkaline-earth iron arsenide (122), etc[1,2]. Among them, the 122 family is the most studied family of iron-based superconductors, due to their high sample quality, high superconducting transition temperature (T_c), tunable carrier density, and diverse compounds with different chemical substitutions. However, despite these advantages, the lattice structure of 122 contains a single alkaline-earth-metal plane and therefore has no charge-neutral cleavage surface (Fig. 1a,b). In $BaFe_2(As_{1-x}P_x)_2$, for example, half Ba ions are removed from the cleavage surface, and the residual Ba ions distribute inhomogeneously, forming various surface terminations[3–7]. While the alkaline-earth-metal-terminated and arsenic-terminated surfaces have been observed by scanning tunneling microscopy (STM)[4–7], the alkaline-earth-metal-deficient surface also exists with a reconstruction of alkaline-earth-metal atoms with 1×2 and $\sqrt{2}\times\sqrt{2}$ periodicities[3,6,7]. In bulk materials, one alkaline-earth-metal plane donates 1.5 electrons equality to the two nearest Fe-As/P planes. However, at the surface, the charge-transfer to the topmost Fe-As/P plane varies depending on the different concentrations of alkaline-earth-metal atoms, leading to a charge-inhomogeneous and charge-non-neutral surface in the 122 iron-based superconductors.

Angle-resolved photoemission spectroscopy (ARPES) is a powerful technique that measures the electronic structure of material in momentum space. In the studies of iron-based superconductors, ARPES plays an important role in determining the band structure, Fermi surface topology, superconducting gap anisotropy, etc[8, 9]. However, as a surface-sensitive technique, ARPES is very sensitive to the cleavage surfaces of materials. In the studies of 1111, the separation of bulk and surface states has been observed, which was attributed to the charge-non-neutral cleavage surface of 1111[10–12]. Meanwhile, for the most studied family of iron-based superconductors, the 122 family, however, its surface complicacy is

rarely considered. While few theories and experiments show possible existences of surface states[3,13], the photoemission spectra is generally much more broadened in 122[13–20] than in other families of iron-based superconductors[21–25]. Such broadening behavior and its origin have not been well understood so far.

Here, we report the measurement of gap anisotropy in an optimal-doped 122 compound $BaFe_2(As_{0.7}P_{0.3})_2$ utilizing ARPES and in-situ potassium deposition. We find that by depositing a small amount of potassium on the sample surface, the spectra become sharp and coherent, which allows us to measure the superconducting gap anisotropy on all Fermi surface sheets of $BaFe_2(As_{0.7}P_{0.3})_2$ with unpreceded precision. Using a single $|\cos k_x \cos k_y|$ gap function, we could well reproduce the gap anisotropy on the outer hole/electron pockets, but not on the inner hole/electron pockets. This indicates that the superconducting pairing is pocket- or orbital-selective in iron-based superconductors, which leads to the existence of two pairing channels originated respectively from the inner and outer Fermi pockets. Our detailed and precise gap measurement provides crucial clues for uncovering the paring mechanism of iron-based superconductors. It also implies that the surface complicacy of 122 need to be seriously considered. The potassium deposition can be used as a practical experiment method for revealing the intrinsic electron structure and gap anisotropy in the future studies of 122 iron-based superconductors.

Results

Evolution of electronic structure in potassium-coated $BaFe_2(As_{0.7}P_{0.3})_2$. The Fermi surface mappings taken in the pristine and doped samples are compared in Fig. 1c,d. The photoemission spectra distribute broadly in the pristine sample (D0). Shadow Fermi pockets could be observed at the Brillouin zone boundary (X), indicating a 1 × 2 reconstruction at the cleavage surface. When depositing with potassium, the sharpening of photoemission spectra is obvious. Two hole pockets (α and β) and two electron pockets (δ and η) are now resolved clearly at the Brillouin zone center (Γ) and zone corner (M). The sharpness of photoemission spectra taken in the doped sample transcends most previous ARPES studies in 122, especially for the Fermi surface mapping around the M point[8,9,14–17]. The sharpness of spectra is now comparable with that in the 11 and 111 iron-based superconductors[21–25]. Note that, the large hole pocket (α_Z) is a shadow pocket that is folded from the Z point due to the finite k_z resolution of ARPES[17].

To further show the effect of potassium deposition, we take the energy-momentum cuts across the hole/electron pockets and plot their doping dependence in Fig. 2. Around the Γ point, the spectra become sharper with potassium deposition, and meanwhile the superconducting peaks become more coherent. Around the M point, a surface band could be observed at around − 20 meV as pointed out by the white arrow (Fig. 2c). With potassium deposition, this surface band weakens and eventually diminishes. As a result, the superconducting coherent peak is clearly resolved in the symmetrized EDCs taken in the D3 sample (Fig. 2d). It should be noted that, the potassium deposition affects mostly the surface electronic state, while leaving the bulk electronic state unaffected[26,27]. As a result, we attribute the sharp spectra to

the bulk electron state, whose Fermi crossings (k_Fs) and superconducting gap magnitudes (Δ) are independent to the potassium deposition.

Superconducting gap anisotropy in potassium-coated $BaFe_2(As_{0.7}P_{0.3})_2$. The superconducting gap anisotropy has been studied extensively in 122 iron-based superconductors, including $Ba(Fe_{1-x}Co_x)_2As_2$[16], $BaFe_2(As_{1-x}P_x)_2$[18], $Ba_{1-x}K_xFe_2As_2$[19,20], etc. If the photoemission spectra consist of both the surface and bulk electronic states, the measured gap magnitude could be inaccurate. Here, the superconducting coherent peaks are well defined in potassium-coated $BaFe_2(As_{0.7}P_{0.3})_2$ on all Fermi surface sheets, which allow us to measure the superconducting gap anisotropy with unpreceded precision. The results are shown in Fig. 3. The superconducting gaps on the α and β hole pockets (Δ_α and Δ_β) are nearly isotropic, while the superconducting gaps on the δ and η electron pockets (Δ_δ and Δ_η) show moderate anisotropy. The gap reaches maximum at 90° for Δ_δ, while for Δ_η, the gap maxima locate at 45° and 135°.

Figure 4 summarizes the angular distributions of the superconducting gap on all Fermi surface sheets. It is commonly believed that the pairing symmetry of 122 is an $s_\pm$-wave[28–31] and the superconducting gap anisotropy can be fitted using a $\Delta_0|\cos k_x \cos k_y|$ gap function[16,18–20]. Here, our detailed and precise gap measurements allow us to test the validity of $s_\pm$ gap function quantitatively. We fitted the data using the experimental determined Fermi surface and a $\Delta_0|\cos k_x \cos k_y|$ gap function. As shown in Fig. 4b-f, for the superconducting gap anisotropies on the β and η pockets, the four-fold gap anisotropy of Δ_η and the relative gap magnitudes of Δ_β and Δ_η can be well described by the $s_\pm$ gap function with Δ_0 = 8.7 meV. However, for the α and δ pockets, the superconducting gap clearly deviates from the $s_\pm$ gap function with larger gap magnitudes, which indicate a stronger superconducting pairing on the α and δ pockets.

Discussion

For a single band superconductor, the superconducting pairing can be normally described using a single pairing channel with a specified symmetry. However, for iron-based superconductors whose Fermi surface consists of multi-bands with multi-orbital characters, the pairing interaction could be complex and consist of multiple pairing channels. Here, we show that the superconducting pairing cannot be described by a single $s_\pm$ pairing channel, but instead consists of at least two pairing channels. One pairing channel follows the $s_\pm$ pairing symmetry and originates from the pair scattering on the β and η pockets. The other pairing channel contributes stronger pairing interactions and originates from the pair scattering on the α and δ pockets.

According to theories, the pair scattering of electrons in iron-based superconductors could be mediated by a large **Q** scattering that connects the Fermi pockets at the Γ and M points[28–31]. On one hand, it has been proposed that the effectivity of the pair scattering is determined by the nesting condition of Fermi surface. Here, the outer hole/electron pockets are similar in size and the inner hole/electron pockets are

well nested. The nesting of Fermi pockets naturally separates out two pair scattering channels, which locate respectively on the outer and inner Fermi pockets. On the other hand, it has been proposed that the pair scattering is most effective when the nesting portions of Fermi surface have the same orbital character[29 – 32]. Here, both the β and η pockets are constructed by the d_{xy} orbital, while the α and δ pockets are constructed by the d_{xz}/ d_{yz} orbitals. The intra-orbital pair scattering leads to a separation of two pairing channels respectively from the d_{xz}/ d_{yz} and d_{xy} orbitals. Based on above discussions, our results suggest that the intra-orbitals pair scattering between two nested Fermi pockets play dominating roles in the superconducting pairing of iron-based superconductors. As a result, the superconducting pairing is pocket- or orbital-selective[32, 33], which explains the deviation from a single $s_{\pm}$ gap function observed here.

Finally, it is intriguing to discuss how the potassium atoms play roles on the surface of $BaFe_2(As_{1-x}P_x)_2$. There are several possible scenarios. First, electrons transfer from the potassium atoms to the sample surface, which neutralizes the charge-non-neutral surface, leading to a suppression of the surface broadening effect. Second, the potassium atoms could act as a catalyzer which causes the redistribution of alkaline-earth metal atoms on the sample surface in a more homogeneous way. Third, the potassium atoms scatter electrons at the sample surface. The surface electronic states then turn into an incoherent and continuous background that is inconspicuous in photoemission spectra. To understand the mechanism of potassium deposition, further experimental and theoretical studies are required. Nevertheless, our results highlight the surface complicacy of 122 iron-based superconductors, which implies that the previous photoemission data taken on 122 should be carefully revisited.

For superconducting gap measurements, previous ARPES studies observed double peak features on both hole and electron pockets in $Ba_{1-x}K_xFe_2As_2$, whose origin remains contraversal[34–37]. Some attribute it to the band degeneracy[34, 35], while others believe it is originated from the electron-bosonic coupling[36] or in-gap impurity state[37]. Here, we show that the surface effect is an alternative explanation of the double peak features and could be verified using the potassium deposition. Improving the accuracy of the superconducting gap measurement could help for refining the theoretical models of iron-based superconductors. On the other hand, for band structure measurements, previous ARPES studies observed complex band structures in $BaFe_2As_2$, $SrFe_2As_2$, $CaFe_2As_2$, etc[38–40]. The number of bands is apparently much larger than the expected number of bands in band calculations. Using potassium deposition, we could distinguish the surface bands from the bulk bands. The results could clarify controversies and help to get a unified picture of the band structure of 122 iron-based superconductors.

In summary, we measured the superconducting gap anisotropy of potassium-coated $BaFe_2(As_{0.7}P_{0.3})_2$ using ARPES. We not only show that the superconducting pairing is pocket- or orbital-selective, but also highlight that the surface complicacy of 122 needs to be seriously considered. Using potassium deposition, we could suppress the surface-broadening effect of 122 and reveal its intrinsic electron properties. Together with all the advantages of 122, the studies of surface-neutralized 122 could provide accurate and crucial clues for uncovering the pairing mechanism of iron-based superconductors.

Methods

Sample preparations. High quality $BaFe_2(As_{0.7}P_{0.3})_2$ single crystals were grown using self-flux method[41]. Ba_2As_3, Ba_2P_3, FeAs, FeP were starting materials, which were mixed at a molar ratio of 2.82 : 0.18 : 0.94 : 0.06, placed in an Al_2O_3 crucible, and sealed in an iron crucible. The crucible was heated at 1150 ℃ for 10 hours, and then the temperature cooled down to 900 ℃ at a rate of 1 ℃ per hour. Finally, 1 mm × 1 mm × 0.2 mm high-quality single crystal can be obtained. The T_c is around 30 K as confirmed by magnetic susceptibility measurement.

Angle-resolved photoemission spectroscopy. The ARPES data were taken at Stanford synchrotron radiation lightsource (SSRL) beamline 5 – 4. The photon energy is 23 eV. The overall energy resolution is around 5 meV and the angular resolution is around 0.3°. The samples were cleaved *in-situ* and measured in vacuum better than 5×10^{-10} mbar. All data were measured at 8 K. The potassium deposition was conducted in-situ using a potassium dispenser. We repeated the deposition several times. The deposition sequence is denoted using Dn (n is the doping times). The current of the potassium dispenser is ~ 5.4 A, and each deposition last for ~ 8 seconds.

Declarations

Data Availability

Data that support the findings of this study are available upon reasonable request from the corresponding authors.

Competing interests

The authors declare no competing interests.

Author contributions

Y. Z. conceived and instructed the project. Z. M. X. synthesized the single crystals. Y. D. W. took the ARPES measurements with the contribution of T. T. H., C. C., Z. G. W., L. C., Z. M. X.. Z. M. X. and Y. Z. analysed the data and wrote the paper with the input from all authors.

Acknowledgements

We gratefully acknowledge the experimental support by Dr. D. H. Lu and Dr. M. Hashimoto at SSRL. This work is supported by the National Natural Science Foundation of China (Grant No. 11888101), the National Key Research and Development Program of China (Grant No. 2018YFA0305602 and No.

2016YFA0301003), and the National Natural Science Foundation of China (No. 91421107 and No. 11574004). Stanford Synchrotron Radiation Lightsource is operated by the Office of Basic Energy Sciences, U.S. Department of Energy.

References

1. Stewart, G. R. Superconductivity in iron compounds. *Rev. Mod. Phy.* 83, 1589–1652 (2011).
2. Paglione, J. & Greene, R. L. High-temperature superconductivity in iron-based materials. *Nat. Phys.* 6, 645–658 (2010).
3. Gao, M., Ma, F., Lu, Z.-Y. & Xiang, T. Surface structures of ternary iron arsenides AFe_2As_2 (A = Ba, Sr, or Ca). *Phys. Rev. B* 81, 193409 (2010).
4. Nascimento, V. B. *et al.* Surface geometric and electronic structure of $BaFe_2As_2$(001). *Phys. Rev. Lett.* 103, 076104 (2009).
5. Yin, J.-X. *et al.* Real space orbital selective probing of the cooper pairing in iron pnictides. Preprint at https://arxiv.org/abs/1602.04949 (2016).
6. Niestemski, F. C. *et al.* Unveiling the atomic and electronic structure at the surface of the parent pnictide $SrFe_2As_2$. Preprint at https://arxiv.org/abs/0906.2761 (2009).
7. Li, A. *et al.* Surface terminations and layer-resolved spectroscopy in 122 iron pnictide superconductors. *Phys. Rev. B* 99, 134520 (2019).
8. Richard, P., Sato, T., Nakayama, K., Takahashi, T. & Ding, H. Fe-based superconductors: an angle-resolved photoemission spectroscopy perspective. *Rep. Prog. Phys.* 74, 124512 (2011).
9. Ye, Z. -R., Zhang, Y., Xie, B. -P. & Feng, D. -L. Angle-resolved photoemission spectroscopy study on iron-based superconductors. *Chin. Phys. B* 22, 087407 (2013).
10. Liu, C. *et al.* Surface-driven electronic structure in LaFeAsO studied by angle resolved photoemission spectroscopy. *Phys. Rev. B* 82, 075135 (2010).
11. Zhang, P. *et al.* Disentangling the surface and bulk electronic structures of LaOFeAs. *Phys. Rev. B* 94, 104517 (2016).
12. Yang, L. X. *et al.* Surface and bulk electronic structures of LaFeAsO studied by angle-resolved photoemission spectroscopy. *Phys. Rev. B* 82, 104519 (2010).
13. Pfau, H. *et al.* Detailed band structure of twinned and detwinned $BaFe_2As_2$ studied with angle-resolved photoemission spectroscopy. *Phys. Rev. B* 99, 035118 (2019).
14. Zhang, Y. *et al.* Orbital characters of bands in the iron-based superconductor $BaFe_{1.85}Co_{0.15}As_2$. *Phys. Rev. Lett.* 83, 054510 (2011).
15. Yi, M. *et al.* Symmetry-breaking orbital anisotropy observed for detwinned $Ba(Fe_{1-x}Co_x)As_2$ above the spin density wave transition. *Proc. Natl. Acad. Sci. U. S. A.* 108, 6878–6883 (2011).
16. Terashima, K. *et al.* Fermi surface nesting induced strong pairing in iron-based superconductors. *Proc. Natl. Acad. Sci. U. S. A.* 106, 7330–7333 (2009).

17. Ye, Z. -R. *et al.* Doping dependence of the electronic structure in phosphorus-doped ferropnictide superconductor $BaFe_2(As_{1-x}P_x)_2$ studied by angle-resolved photoemission spectroscopy. *Phys. Rev. B* 86, 035136 (2012).
18. Zhang, Y. *et al.* Nodal superconducting-gap structure in ferropnictide superconductor $BaFe_2(As_{0.7}P_{0.3})_2$. *Nat. Phys.* 8, 371–375 (2012).
19. Ding, H. *et al.* Observation of Fermi-surface-dependent nodeless superconducting gaps in $Ba_{0.6}K_{0.4}Fe_2As_2$. *Europhys. Lett.* 83,470031 (2008).
20. Nakayama, K. *et al.* Superconducting gap symmetry of $Ba_{0.6}K_{0.4}Fe_2As_2$ studied by angle-resolved photoemission spectroscopy. *Europhys. Lett.* 85, 67002 (2009).
21. Watson, M. D. *et al.* Evidence for unidirectional nematic bond ordering in FeSe. *Phys. Rev. B* 94, 201107 (2016).
22. Zhang, Y. *et al.* Distinctive momentum dependence of the band reconstruction in the nematic state of FeSe thin film. *Phys. Rev. B* 94, 115153 (2016).
23. Miao, H. *et al.* Isotropic superconducting gaps with enhanced pairing on electron Fermi surfaces in $FeTe_{0.55}Se_{0.45}$. *Phys. Rev. B* 85, 094506 (2012).
24. Borisenko, S. V. *et al.* Superconductivity without nesting in LiFeAs. *Phys. Rev. Lett.* 105, 067002 (2010).
25. Umezawa, K. *et al.* Unconventional anisotropic s-wave superconducting gaps of the LiFeAs iron-pnictide superconductor. *Phys. Rev. Lett.* 108, 037002 (2012).
26. Seo, J. J. *et al.* Superconductivity below 20 K in heavily electron-doped surface layer of FeSe bulk crystal. *Nat. Commun.* 7,11116 (2016).
27. Riley, J. M. *et al.* Negative electronic compressibility and tunable spin splitting in WSe_2. *Nat. Nano.* 10, 1043–1048 (2015).
28. Hirschfeld, P. J., Korshunov, M. M. & Mazin, I. I. Gap symmetry and structure of Fe-based superconductors. *Rep. Prog. Phys.* 74, 124508 (2011).
29. Wang, F. & Lee, D. -H. The electron-pairing mechanism of iron-based superconductors. *Science*. 332, 200–204 (2011).
30. Dai, P., Hu, J. & Dagotto, E. Magnetism and its microscopic origin in iron-based high-temperature superconductors. *Nat. Phys.* 8, 709–718 (2012).
31. Mazin, I. I. & Schmalian, J. Pairing symmetry and pairing state in ferropnictides: theoretical overview. *Phys. C.* 469,614–627 (2009).
32. Sprau, P. O. *et al.* Discovery of orbital-selective Cooper pairing in FeSe. *Science*. 357, 75–80 (2017).
33. Kreisel, A. *et al.* Orbital selective pairing and gap structures of iron-based superconductors. *Phys. Rev. B* 95, 174504 (2017).
34. Xu, Y. -M. *et al.* Observation of a ubiquitous three-dimensional superconducting gap function in optimally doped $Ba_{0.6}K_{0.4}Fe_2As_2$. *Nat. Phys.* 7, 198–202(2011).

35. Zhang, Y. *et al.* Out-of-plane momentum and symmetry-dependent energy gap of the pnictide $Ba_{0.6}K_{0.4}Fe_2As_2$ superconductor revealed by angle-resolved photoemission spectroscopy. *Phys. Rev. Lett.* 105, 117003 (2010).
36. Shimojima, T. *et al.* Anomalous two peak structure in the Angle-resolved Photoemission Spectra of $Ba_{1-x}K_xFe_2As_2$. Preprint at https://arxiv.org/abs/1206.3163 (2012).
37. Zhang, P. *et al.* Observation of momentum-confined in-gap impurity state in $Ba_{0.6}K_{0.4}Fe_2As_2$: evidence for anti-phase $s_{\pm}$ pairing. *Phys. Rev. X* 4, 031001(2014).
38. Yi, M. *et al.* Unconventional electronic reconstruction in undoped (Ba, Sr) Fe_2 As_2 across the spin density wave transition. *Phys. Rev. B* 80, 174510 (2009).
39. Zhang, Y. *et al.* Unusual doping dependence of the electronic structure and coexistence of spin-density-wave and superconductor phases in single crystalline $Sr_{1-x}K_xFe_2As_2$. *Phys. Rev. Lett.* 102, 127003 (2009).
40. Wang, Q. *et al.* Uniaxial "nematic-like" electronic structure and Fermi surface of untwinned $CaFe_2As_2$. Preprint at https://arxiv.org/abs/1009.0271 (2010).
41. Nakajima, M. *et al.* Growth of $BaFe_2(As_{1-x}P_x)_2$ single crystals ($0 \leq x \leq 1$) by Ba_2As_3/Ba_2P_3-flux method. *J. Phys. Soc. Japan.* 81, 104710 (2012).

Figures

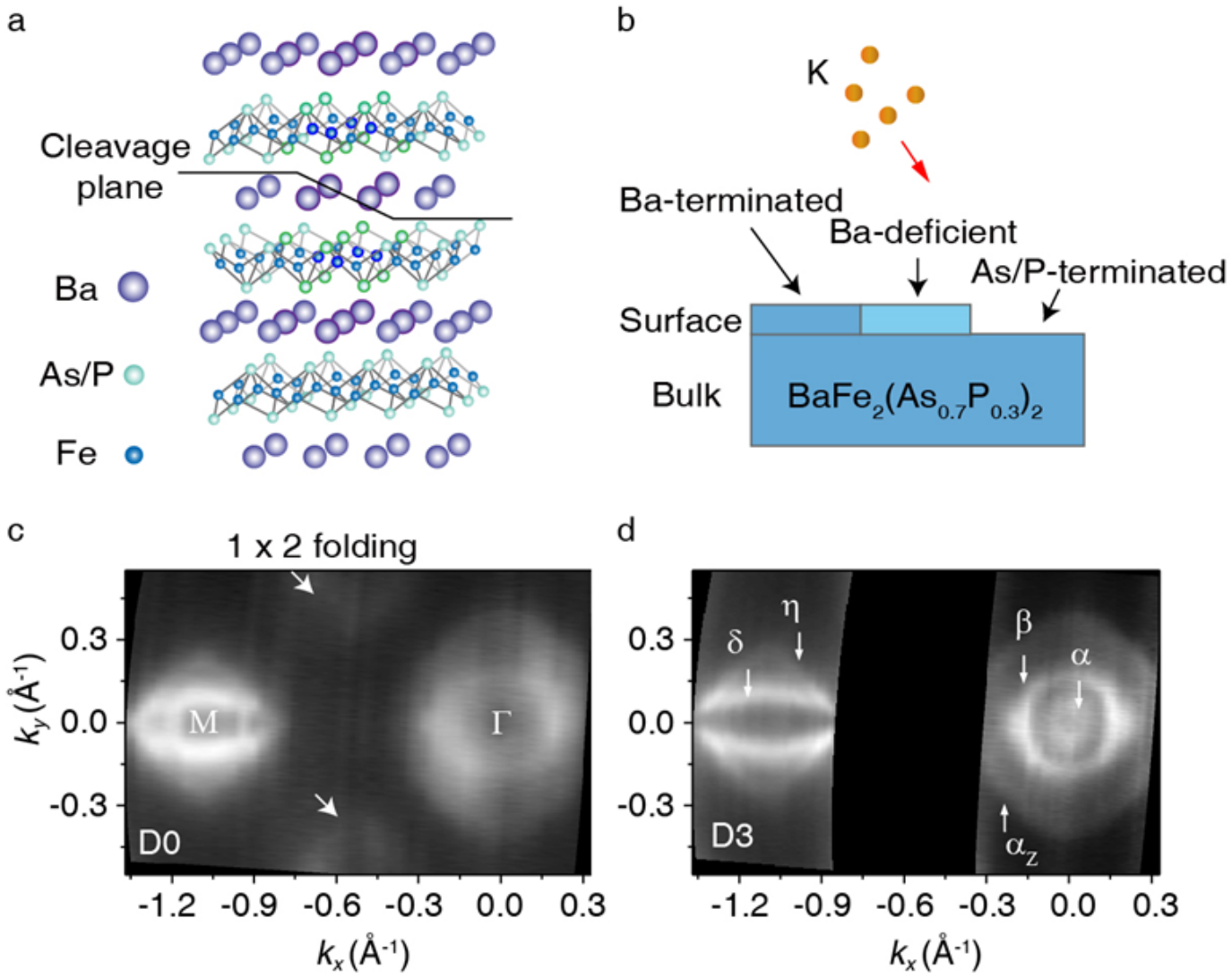

Figure 1

Surface complicacy of BaFe2(As0.7P0.3)2 a Schematic drawing of the lattice structure of BaFe2(As0.7P0.3)2. The black solid line illustrates the position of the cleavage plane. b Schematic drawing of the cleavage surface and potassium deposition. c Fermi surface mapping taken in the pristine sample (D0). d is the same as panel c but taken in doped sample after three times potassium deposition (D3).

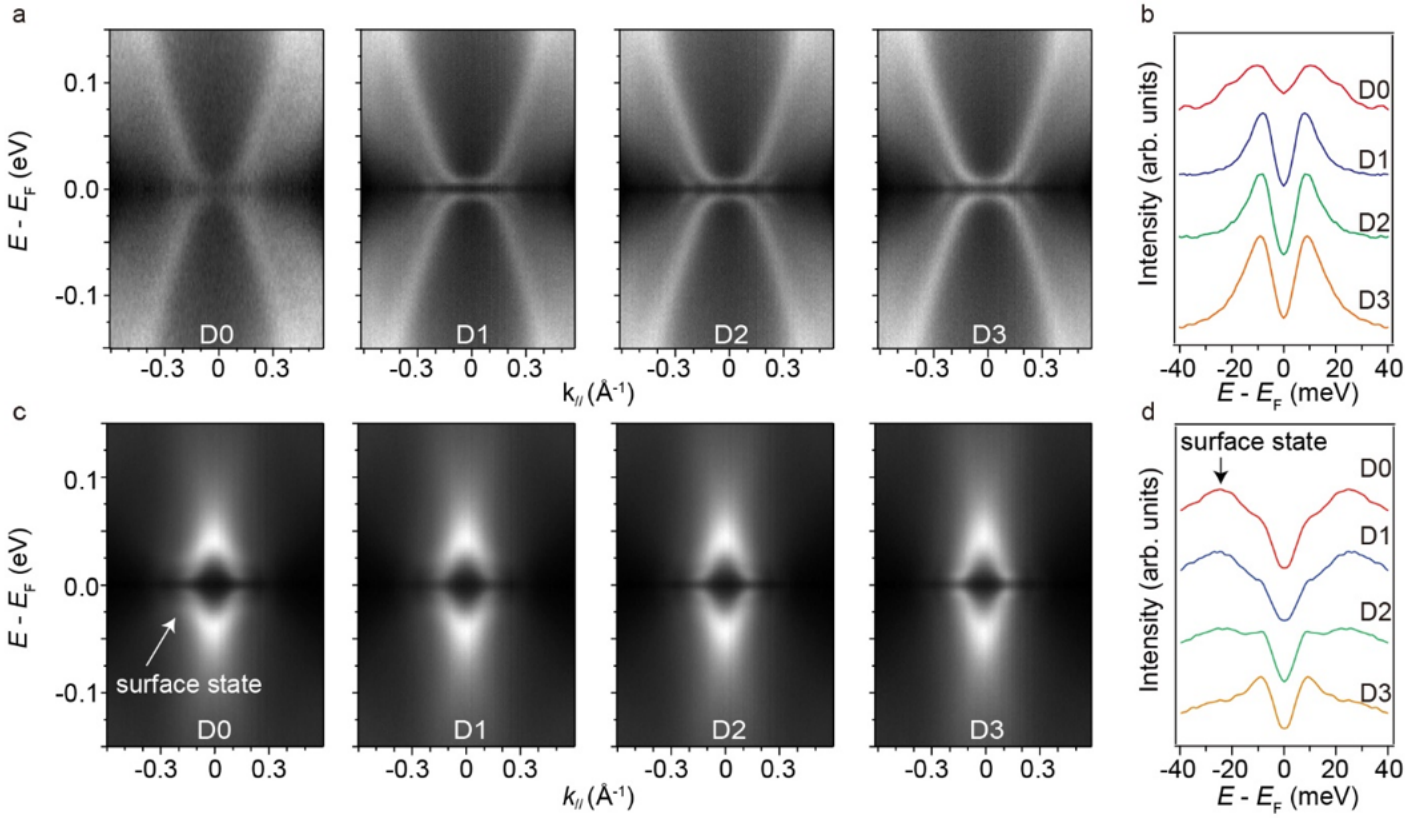

Figure 2

Band evolution in potassium-coated BaFe2(As0.7P0.3)2. a Doping dependence of the symmetrized energy-momentum cuts taken around the Γ point. b Doping dependence of the symmetrized energy distribution curves (EDCs) taken at the Fermi crossing (kF) of the α hole band. c and d are the same as panels a and b but taken around the M point. The EDCs are taken at the kF of the δ electron band. The deposition sequence is denoted using Dn (n is the doping times).

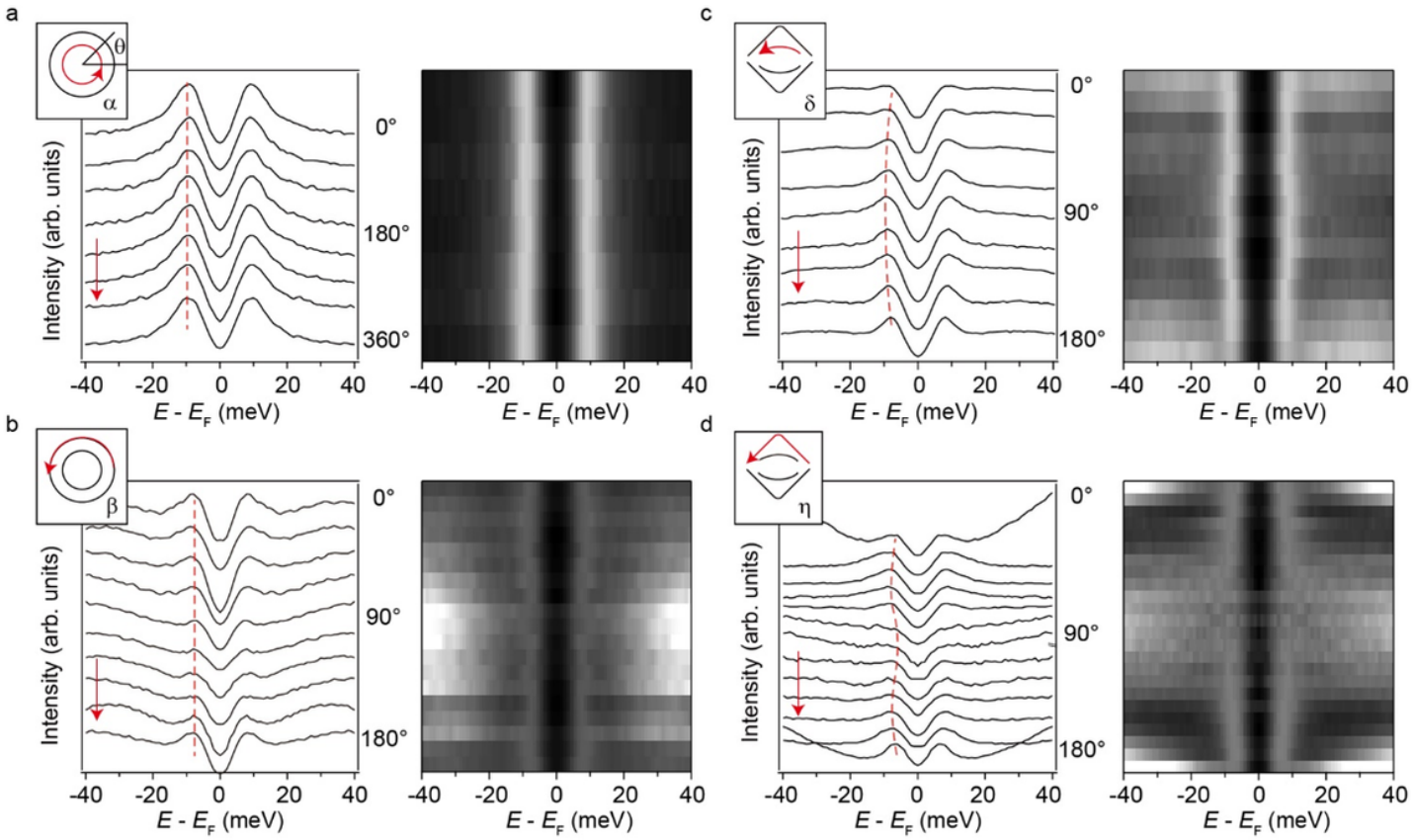

Figure 3

Angular distributions of superconducting gap on Fermi surface sheets. a Angle dependence of the symmetrized EDCs taken on the α hole pocket. The red dashed line guides the eyes to the gap anisotropy. The right panel is a merged image of the symmetrized EDCs for better visualizing the gap anisotropy. b, c, and d are the same as panel a, but taken on the β, δ, and η pockets respectively. All data were taken in the D3 sample at 8 K.

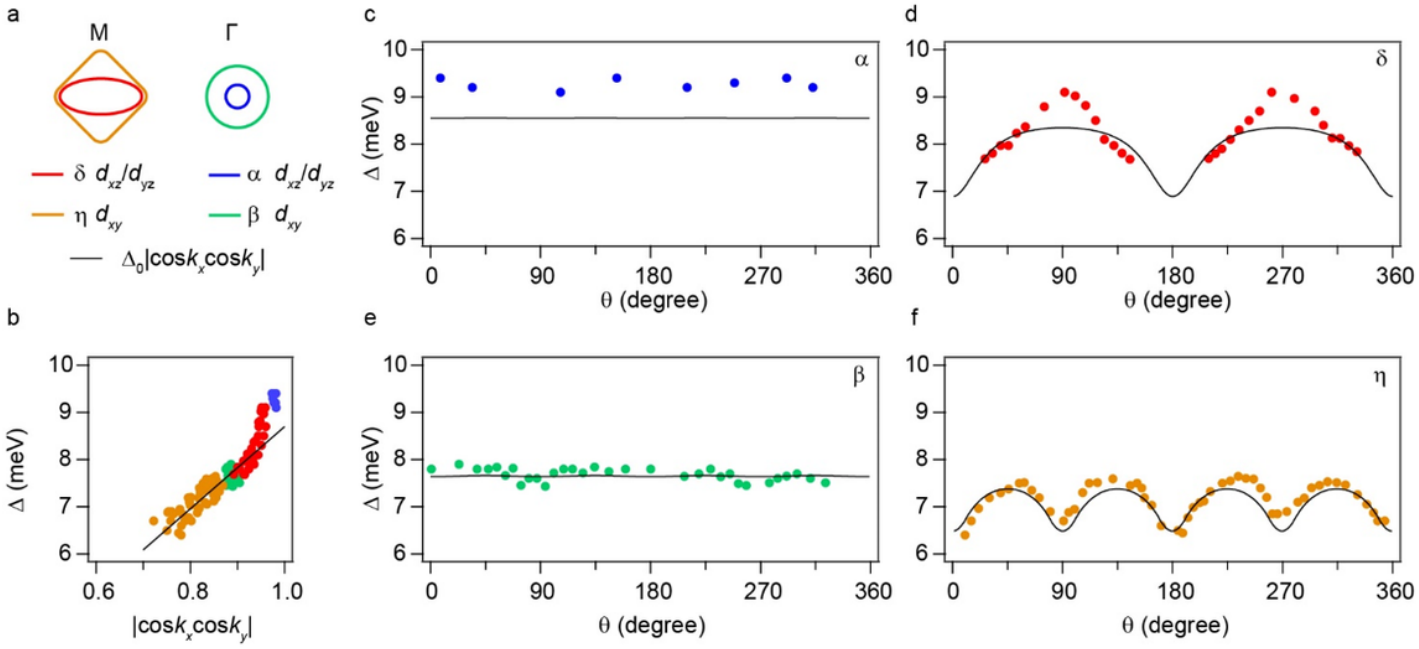

Figure 4

Superconducting gap fitting using an s± gap function. a Schematic drawing of the Fermi surface of BaFe2(As0.7P0.3)2. b Plot of the superconducting gap as a function of |coskxcosky|. c Angular distribution of the superconducting gap on the α pocket. d, e, and f are the same as panel c but taken on the β, δ, and η pockets respectively. The black solid lines in all panels are the best fit using the gap function Δ0|coskxcosky| with Δ0 = 8.7 meV.